



**HAL**  
open science

## Optimizing magneto-optical effects in the ferromagnetic semiconductor GaMnAs

Hassen Riahi, L. Thevenard, Mhamed Ali Maaref, Bruno Gallas, Aristide Lemaître, Catherine Gourdon

► **To cite this version:**

Hassen Riahi, L. Thevenard, Mhamed Ali Maaref, Bruno Gallas, Aristide Lemaître, et al.. Optimizing magneto-optical effects in the ferromagnetic semiconductor GaMnAs. *Journal of Magnetism and Magnetic Materials*, 2015, 395, pp.340 - 344. 10.1016/j.jmmm.2015.07.090 . hal-01444949

**HAL Id: hal-01444949**

**<https://hal.science/hal-01444949>**

Submitted on 24 Jan 2017

**HAL** is a multi-disciplinary open access archive for the deposit and dissemination of scientific research documents, whether they are published or not. The documents may come from teaching and research institutions in France or abroad, or from public or private research centers.

L'archive ouverte pluridisciplinaire **HAL**, est destinée au dépôt et à la diffusion de documents scientifiques de niveau recherche, publiés ou non, émanant des établissements d'enseignement et de recherche français ou étrangers, des laboratoires publics ou privés.

# Optimizing magneto-optical effects in the ferromagnetic semiconductor GaMnAs

H.Riahi<sup>a\*</sup>, L. Thevenard<sup>b,c</sup>, M. A. Maaref<sup>a</sup>, B. Gallas<sup>b,c</sup>, A. Lemaître<sup>d</sup>, C. Gourdon<sup>b,c</sup>  
<sup>a</sup> *Laboratoire Matériaux Molécules et Applications, IPEST, Université de Carthage, La Marsa, Tunisie*

<sup>b</sup> *CNRS, UMR7588, Institut des Nanosciences de Paris, 4 place Jussieu, 75005 Paris, France*

<sup>c</sup> *Sorbonne Universités, UPMC Université Paris 06, UMR7588, 4 place Jussieu, 75005 Paris, France.*

<sup>d</sup> *Laboratoire de Photonique et de Nanostructures – CNRS, Route de Nozay, 91460 Marcoussis, France.*

*e-mail: hassenriahi1987@gmail.com*

*Keywords : magnetic semiconductors, magneto-optical Kerr effect*

## Abstract:

A trilayer of the ferromagnetic semiconductor GaMnAs, a SiO<sub>2</sub> buffer layer and a piezoelectric ZnO layer, is investigated in view of its use in device implementation to study surface acoustic wave-assisted magnetization switching. The magneto-optical properties: Kerr rotation and ellipticity and magnetic contrast in Kerr microscopy images are investigated as a function of temperature. While the ZnO layer prevents any good quality imaging of magnetic domains, we show that with the SiO<sub>2</sub> layer only the polar Kerr rotation and the magnetic contrast are increased by a factor of 2. This result is in good quantitative agreement with calculations using an optical interference model and could be further improved. The detrimental effects of the dielectric layers capping on the Curie temperature and coercive field of the GaMnAs layer can be kept to a reasonable level.

## 1. Introduction :

The ferromagnetic semi-conductor (Ga,Mn)As has received considerable attention in the recent years, as a promising material for future semiconductor spintronic devices [1,2]. It has become a test-bed material for magnetization manipulation by static strain [3,4], electric field [5], light pulses [6, 7, 8, 9], acoustic (strain) pulses [10, 11], and very recently by surface acoustic waves (SAW) [12,13]. This has been made possible thanks to the large sensitivity of the magnetic anisotropy to strain [14, 15]. Strain waves like SAWs have been identified as a powerful tool for magnetization switching in magneto-strictive materials [16, 17, 18]. In GaMnAs, it was recently demonstrated that magnetization precession can be resonantly driven by a SAW when both the magnon and phonon frequencies match [13], which is the first necessary step towards precessional switching [12]. The most direct evidence for magnetization switching can be obtained from magneto-optical imaging using Kerr microscopy (KM) based on the rotation of the linear polarization of light upon reflection on a magnetized sample [19, 20]. However, the Kerr

rotation angle is usually no more than a fraction of degree in GaMnAs [21]. Therefore, differential imaging and an exposure time of the order of 1 s have to be used [22]. It is well known that this rotation angle and thus the magnetic contrast can be enhanced by using multiple reflections in an additional anti-reflecting dielectric layer deposited onto the surface of metallic magnetic samples [19, 23, 24, 25]. However, this has not yet been evidenced with magnetic semiconductors in which the typical penetration depth of light can be of several hundreds of nm. Dielectric layers are also needed for SAW generation and detection. Since GaMnAs is weakly piezoelectric, interdigitated metallic transducers combs for SAW generation and detection need to be patterned onto a piezoelectric ZnO layer evaporated at high temperature (150-250°C) on GaMnAs with a SiO<sub>2</sub> buffer layer. However, this process might be detrimental since the magnetic properties of the GaMnAs layer highly depend on strain and heat treatment [22].

The point is then to take advantage of these dielectric layers to optimize the magnetic contrast while keeping the detrimental effect of this capping as low as possible.

In this paper, we investigate the wavelength and temperature dependence of the magneto-optical properties of a GaMnAs layer with and without capping by dielectric layers using polar magneto-optical Kerr effect (PMOKE).

## 2 - Sample and experimental setup

The sample is a 50 nm thick Ga<sub>1-x</sub>Mn<sub>x</sub>As (x= 0.07) layer grown on a (Ga,In)As relaxed buffer layer deposited on a semi-insulating (001) GaAs substrate in order to achieve perpendicular magnetic easy axis [22,26]. The (Ga,Mn)As layer was deposited at 250 ° C. After the growth, the sample was thermally annealed at 250°C for 1 hour in order to improve its magnetic properties.

From SQUID magnetometry the Curie temperature was found to be 116 K and the active Mn concentration was about 3.3 %. One sample was kept as a reference (GaMnAs-ref). On one part of the second sample (named GaMnAs/SiO<sub>2</sub>/ZnO) a SiO<sub>2</sub>(80 nm)/ZnO (250nm) bilayer was grown by radio-frequency sputtering. The rest of the sample was masked during the growth of the dielectric layers. Care was taken to keep the sample holder at relatively low temperature (150°C) in order not to further anneal the GaMnAs layer. The masked GaMnAs part (GaMnAs-h) is nevertheless checked. After optical investigation, the ZnO layer was removed with HCl leaving a GaMnAs/SiO<sub>2</sub> part. Eventually, SiO<sub>2</sub> was further removed by hydrofluoric acid.

MOKE measurements were performed in the polar geometry with the light beam at quasi-normal incidence on the sample surface. Monochromated light from a 150 W Xe lamp was polarized with a Glan-Thompson polarizer, chopped at  $f_0=250$  Hz by a mechanical chopper and phase-modulated at  $f=50$  kHz by a photo-elastic modulator (PEM). The beam reflected off the sample passed through an analyzer, and was detected by a Si photodiode whose signal was fed into lock-in amplifiers. The signal at  $f_0$  provided a measurement of the average light intensity at each wavelength. The Kerr rotation angle  $\theta_K$  and the ellipticity  $\eta_K$  were obtained from the signals at  $2f$  and  $f$ , respectively, following the procedure described in Ref. [27]. The sample was kept in a helium-flow cryostat, allowing the temperature  $T$  to be varied from 10 to 300 K. An external magnetic field was applied perpendicular to the sample surface and could be swept between  $-20$  mT and  $+20$  mT. The KM images were obtained using a polarizing microscope in reflection geometry. The sample was illuminated at  $\lambda= 670$  nm, close to the maximum of the Kerr rotation angle. Hysteresis cycle can be obtained by averaging the signal over each image while scanning the magnetic field. Details can be found elsewhere [22].

### 3- Results and discussion

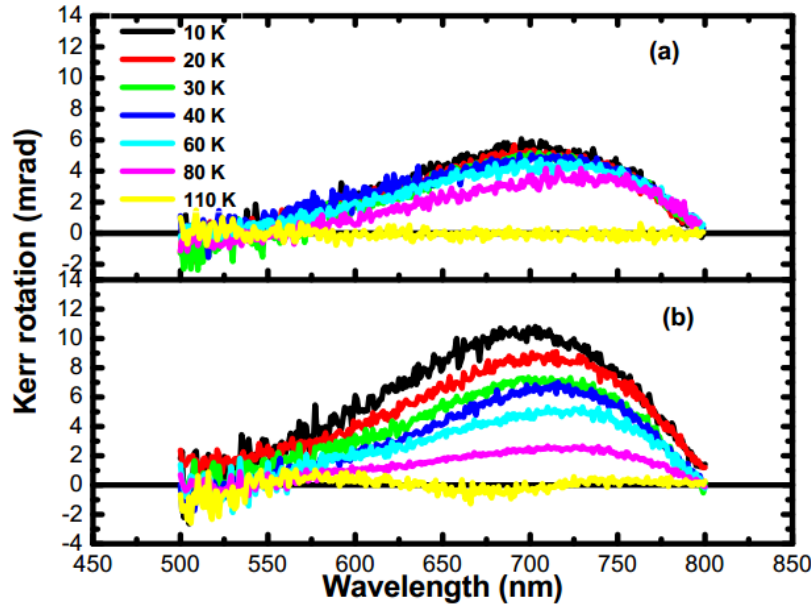


Fig.1. Kerr rotation spectra at different temperatures for GaMnAs (a) and GaMnAs/SiO<sub>2</sub> (b) layers.

First, samples GaMnAs-ref, GaMnAs-h, and GaMnAs/SiO<sub>2</sub>/ZnO were studied. Hysteresis cycles were obtained from KM images at  $T=30$  K. The first two samples show very similar hysteresis cycles. The coercive field was the same (2.5 mT) however the saturation field was larger for GaMnAs-h indicating that the heating process has created defects acting as domain-wall pinning centers. The coercive field was slightly larger for GaMnAs/SiO<sub>2</sub>/ZnO (3.3 mT instead of 2.5 mT), so was the saturation field. In this sample, the magnetic contrast between the up and down magnetized states is similar to GaMnAs-h however the details of the magnetic domains pattern could hardly be distinguished. These results mean that in future SAW devices, the ZnO layer will have to be removed between the generating and detecting interdigitated combs in order to allow magneto-optical imaging of domains in the GaMnAs layer. We will therefore now concentrate on the magneto-optical properties of the different zones of the sample after ZnO removal, namely GaMnAs/SiO<sub>2</sub> and GaMnAs-h, hereafter simply called GaMnAs.

PMOKE spectra are shown in Fig. 1 for GaMnAs/SiO<sub>2</sub> and GaMnAs. For both zones, the spectral dependence of the Kerr rotation  $\theta_K$  is similar with a maximum around 704 nm. It is clear that the Kerr rotation is enhanced by a factor 2 at  $T=10$  K for GaMnAs/SiO<sub>2</sub> with respect to GaMnAs. Such an effect, which will be discussed in more details in the next section, was already observed for other ferromagnetic materials (TbFe and GdT<sub>2</sub>FeCo with a-Si:0 [23], NiFe with ZnS [24]). MgO and SiN<sub>x</sub> capping layers on CoFe have also been investigated [25].

The amplitude of  $\theta_K$  decreases with temperature. This point will be addressed more quantitatively below.

Figure 2 shows the ellipticity  $\eta_K$  versus wavelength for both samples at  $T=10$  K. Both spectra have the same energy dip, at about 760 nm. This dip is at lower energy relative to

the  $\theta_K$  peak. The ellipticity (in absolute value) is larger than the Kerr rotation (about 20 mrad at the dip position) however the enhancement with the SiO<sub>2</sub> layer is not as high as for the Kerr rotation (21 mrad instead of 18 mrad at the dip position) in agreement with calculations (see below).

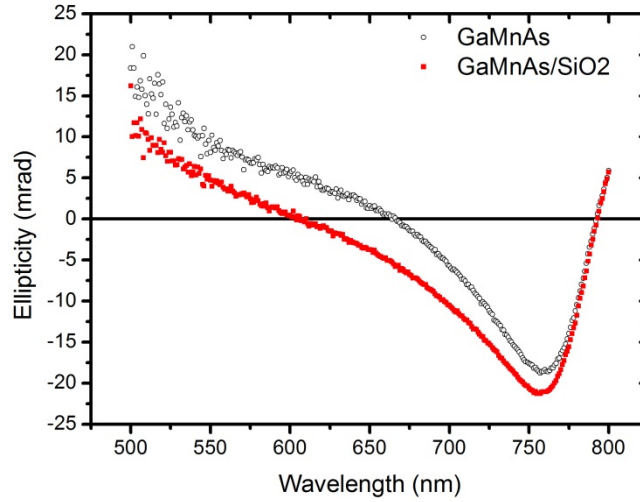


**Fig.2.** Ellipticity as a function of wavelength at  $T=10$  K for GaMnAs (black empty circles) and GaMnAs/SiO<sub>2</sub> (red squares).

In order to assess the usefulness of the SiO<sub>2</sub> capping layer in the operating conditions for SAW devices we take Kerr images of the magnetic domains at different temperatures from  $T=30$  K to  $T=90$  K for GaMnAs/SiO<sub>2</sub> and GaMnAs layers (Fig.3).

In each image of Fig. 3, the GaMnAs and GaMnAs/SiO<sub>2</sub> zones are on the left and right parts of the image, respectively, as delimited by the dashed line. The sample edge is shown by the full line. These images are differential images. The reference is taken with the magnetization fully saturated in one direction. Therefore, the reversed domains appear on a uniform background. As typically observed for GaMnAs grown on a GaInAs pseudo-substrate [22], magnetization reversal proceeds with the nucleation and growth of dendritic like domains branching along the [110] and [-110] crystallographic directions. The contrast between the up and down states of magnetization is defined as

$C=2(I_+-I_-)/(I_++I_-)$  where  $I_+$  and  $I_-$  are the intensities of up and down magnetized domains, respectively. At  $T=31$  K domains appear as much brighter for GaMnAs/SiO<sub>2</sub>. The magnetic contrast is enhanced from 5.6 % to 11.3 %, i.e. by a factor of 2, with the SiO<sub>2</sub> capping layer on GaMnAs. However, the nucleation of domains and their expansion is more difficult, in agreement with the slightly larger coercive field and higher field needed to reach saturation. At higher temperature, domain nucleation occurs at the sample edge and propagation is not impeded.

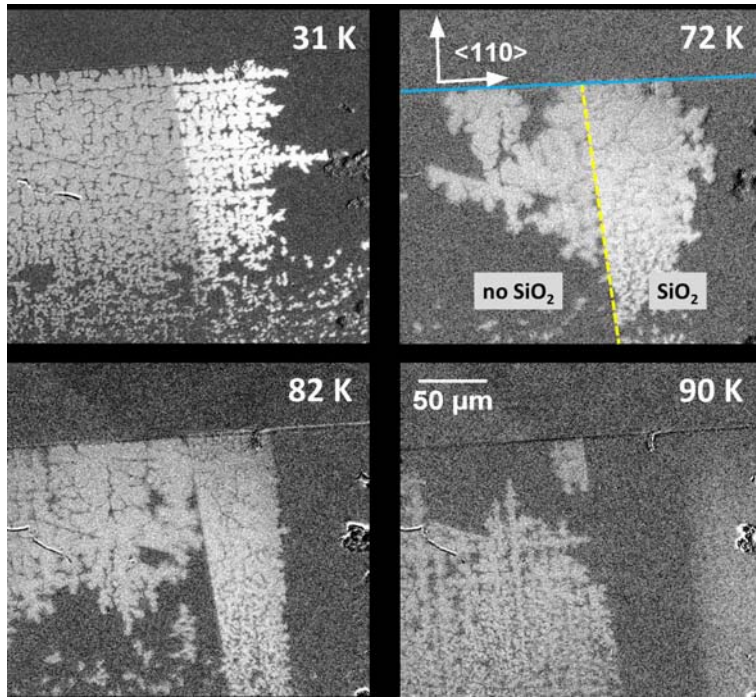


Fig.3. Snapshots of the magnetic domain structure observed by KM in a temperature range 30 K - 90 K, on the GaMnAs layer with and without SiO<sub>2</sub> capping layer (right and left side of the dashed line, respectively). The sample edge is shown by a full line. Here, the magnetic contrast has been digitally enhanced with respect to the original images for the sake of clarity

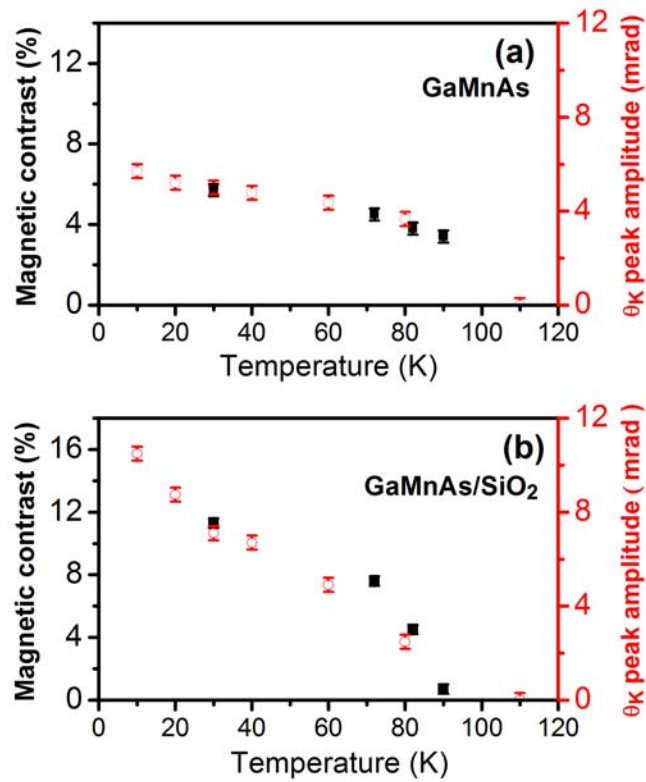


Fig.4. Dependence of the Kerr rotation peak amplitude (open circles) and the magnetic contrast of Kerr images (solid squares) on the temperature for GaMnAs (a) and GaMnAs/SiO<sub>2</sub> (b) layers.

Figure 4 shows the magnetic contrast of Kerr images together with the peak of the Kerr rotation angle obtained from PMOKE as a function of temperature for GaMnAs (Fig. 4 (a)) and GaMnAs/SiO<sub>2</sub> (Fig. 4 (b)). The magnetic contrast follows the same temperature dependence as the Kerr rotation. The proportionality factors between the contrast and the Kerr angle are not exactly identical for GaMnAs and GaMnAs/SiO<sub>2</sub> but close (1.2 and 1.5, respectively), although they should theoretically be equal in our experimental conditions. For GaMnAs/SiO<sub>2</sub>, the contrast drops to zero at  $T=90$  K, indicating a reduction of the Curie temperature from 116 K to 90 K. A similar drop of  $T_C$  has also been found from electrical measurements of the SAW attenuation and velocity change in a SAW-driven ferromagnetic resonance experiment in GaMnAsP [13]. After full removal of the SiO<sub>2</sub> layer,  $T_C$  remains at 93 K indicating that irreversible damages were produced as could also be found from X-rays measurements on a similar sample [13].

#### 4- Model

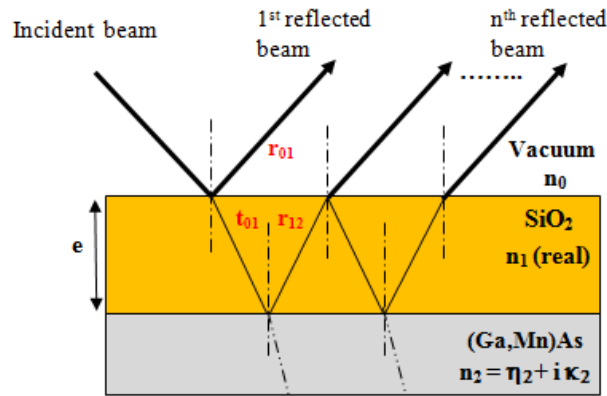


Fig.5. Schematic illustration of a model based on optical interferences in (Ga,Mn)As/SiO<sub>2</sub> structure. For the sake of clarity, the experimentally near-normal incidence light beam is shown here with a large incidence angle.

The experimental results will be discussed in the framework of an optical interference model as schematically depicted in Fig. 5. We assume that the GaMnAs layer has an infinite thickness, *i.e.* we do not take into account reflection at the substrate interface, which is weak owing to a very small difference of refractive indices [11]. The refractive index  $n_1$  (real) of the silica layer is taken from [28]. The wavelength dependence of the real and imaginary parts of the GaMnAs refractive index  $n_2 = \eta_2 + i\kappa_2$  are obtained from ellipsometry measurements on a similar sample at room temperature. The amplitude reflection coefficient at normal incidence is written as:

$$r = \frac{r_{01} + r_{12} \exp(i t e)}{1 + r_{01} r_{12} \exp(i t e)} \quad (1)$$

where  $r_{01}=(1-n_1)/(1+n_1)$  and  $r_{12}=(n_1-n_2)/(n_1+n_2)$  are the amplitude reflection coefficients at the vacuum/SiO<sub>2</sub> interface and at the SiO<sub>2</sub>/GaMnAs interface respectively.  $e$  is the SiO<sub>2</sub> thickness and  $t$  is equal to  $4\pi n_1/\lambda$  with  $\lambda$  the wavelength. It is expected that in the condition of anti-reflection, i.e. for a silica thickness close to a quarter of the wavelength in this material  $\lambda/(4n_1)$ , multiple reflections at the silica/GaMnAs interface will enhance the Kerr rotation while decreasing the intensity of reflected light.

By minimizing the reflectance  $R=rr^*$ , one deduces the expression of the optimal thickness of the SiO<sub>2</sub> layer:

$$e_{opt} = \frac{\lambda}{2\pi n_1} \text{ArcTan} \left( \frac{\text{Re}(r_{12}) - |r_{12}|}{\text{Im}(r_{12})} \right) \approx \frac{\lambda}{2\pi n_1} \text{ArcTan} \left( \frac{\eta_2^2 - n_1^2}{n_1 \kappa_2} \right) \quad (2)$$

where Re (Im) denotes the real (imaginary) part, respectively, and the approximate expression assumes a weak absorption in GaMnAs ( $\kappa_2 \ll (\eta_2, n_1)$ ). The optimal thickness shown in the inset of Fig. 6, is found to be within a few percent (4.5 % to 1.8 %) of the quarter wavelength  $\lambda/(4n_1)$  in the spectral range  $\lambda=500$  nm to 800 nm.

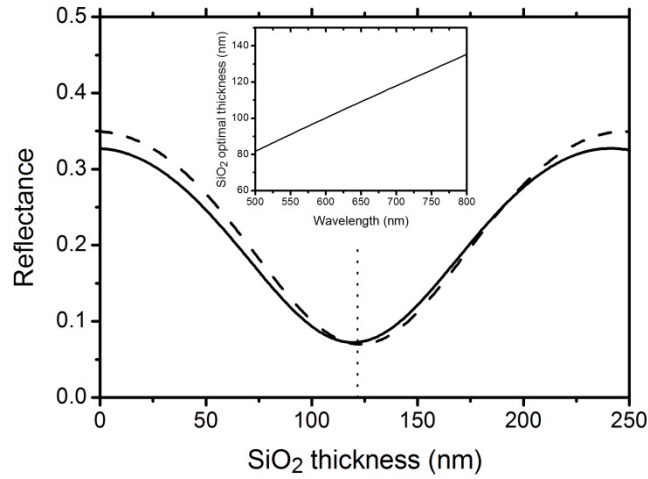


Fig. 6. Reflectance as a function of SiO<sub>2</sub> thickness at the peak of Kerr rotation ( $\lambda=704$  nm), for normal incidence (full line) and 20° incidence (dashed line). The dotted vertical line shows the value of the SiO<sub>2</sub> thickness equal to a quarter wavelength in the SiO<sub>2</sub> layer  $e=\lambda/(4n_1)$ . The inset shows the SiO<sub>2</sub> thickness for minimum reflectance as a function of the wavelength (Eq. 2).

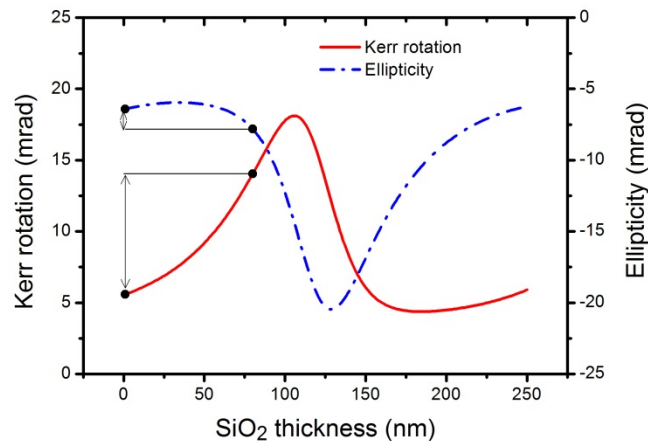


Fig. 7. Kerr rotation angle (solid line) and ellipticity (dashed-dotted line) at 704 nm (peak of the Kerr rotation) and  $T=10$  K as a function of the SiO<sub>2</sub> thickness from Eq. 3. The arrows show the change of Kerr rotation and ellipticity from no SiO<sub>2</sub> layer to a 80 nm SiO<sub>2</sub> layer.

The calculated reflectance is shown in Fig. 6 at  $\lambda=704$  nm (the peak of Kerr rotation) as a function of the silica thickness. The reflectance minimum is broad. The choice of the SiO<sub>2</sub> thickness is therefore not critical. The thickness for minimum reflectance is 119 nm. The reflectance has also been calculated for an angle of incidence of 20° (the maximum incidence angle with the microscope objective used for KM). It is shown by the dashed line in Fig. 6. There is minor change with respect to normal incidence; which means that optimization of the silica thickness can be done without taking into account the numerical aperture of the objective.

The Kerr rotation and ellipticity are calculated as  $Re(\Theta_K)$  and  $Im(\Theta_K)$ , respectively, where  $\Theta_K$  reads:

$$\Theta_K = -i \frac{Q(r_{01}^2 - 1)(1 + r_{12})t_{21} \exp(i t e)}{4(r_{01} + r_{12} \exp(i t e))(1 + r_{01} r_{12} \exp(i t e))} \quad (3)$$

where  $Q = Q_r + iQ_i$  is the complex Kerr coefficient proportional to the saturation magnetization  $M$ . It is related to the off-diagonal element  $\varepsilon_{xy}$  of the dielectric permittivity tensor by  $\varepsilon_{xy} = -i\varepsilon_2 Q m_z$ , with  $m_z$  the component of the unit magnetization vector along the normal to the sample surface and  $\varepsilon_2 = n_2^2$  [19]. The transmission coefficient  $t_{21}$  is equal to  $2n_2/(n_1 + n_2)$ .

The  $Q_r$  and  $Q_i$  values are obtained from the experimental Kerr rotation and ellipticity at  $T=10$  K. The dependence of the Kerr rotation and ellipticity on the SiO<sub>2</sub> thickness at the peak of Kerr rotation  $\lambda=704$  nm is calculated and shown in Fig. 7. The arrows show the change of Kerr rotation and ellipticity from zero to 80 nm of silica. They are in good agreement with experimental results. One finds a change of the Kerr rotation from 5.6 mrad to 14 mrad (10.5 mrad experimentally) and of the ellipticity from -6.4 mrad to -7.8 mrad (-11 mrad experimentally). In particular, the increase of the Kerr rotation is larger than the increase of Kerr ellipticity (in absolute value), as found experimentally. The precise knowledge of the GaMnAs refractive index at low temperature would certainly improve the agreement with experimental results. One can note that the peak of Kerr rotation is found for a silica thickness of 106 nm, slightly smaller than the thickness for minimum reflectance (119 nm).

## 5- Conclusion:

In view of using dielectric SiO<sub>2</sub> and ZnO layers as buffer layer and piezoelectric transducer, respectively, for surface acoustic wave generation and detection on a ferromagnetic semiconductor, we have grown a GaMnAs/SiO<sub>2</sub>/ZnO sandwich and studied its magneto-optical properties. The aim was to assess the possible detrimental changes of the magnetic properties after the growth of overlayers on the GaMnAs ferromagnetic layer and to improve magneto-optical imaging for the study of SAW-assisted magnetization reversal. Although the magnetic properties of the tri-layer were not seriously altered, the ZnO layer did not allow good quality imaging of the magnetic domains. In future SAW devices, the ZnO layer will have to be removed in a window between the two sets of excitation and detection interdigitated combs. With a SiO<sub>2</sub> layer of 80 nm, the magnetic

contrast could be multiplied by 2. An optimized thickness of 106 nm should further increase the contrast. The temperature behavior of the magnetic contrast and the Kerr rotation angle has shown that the Curie temperature decreased from 116 K to 90 K with the SiO<sub>2</sub> capping layer. This remains a problem but not too serious for SAW device operation. More generally this work can serve as a basis for optimization of magnetic contrast in magnetic semiconductors, not only for the investigation of SAW induced magnetization switching but also for the study of domain patterns and domain wall dynamics.

#### Acknowledgement

We are grateful to J. Y. Duquesne from Institut des Nanosciences de Paris for the growth of the dielectric layers on GaMnAs. This work has been supported by Region Ile-de-France (DIM Nano-K MURAS2012), by Agence Nationale de la Recherche (ANR 2010-BLANC-0424-02 and ANR13-JS04-0001-01), and by the French RENATECH network. One of us, H. R., acknowledges financial support from the Ministry of Higher Education and Scientific Research of Tunisia.

- [1] P. Němec, V. Novák, N. Tesařová, E. Rozkotová, H. Reichlová, D. Butkovičová, F. Trojánek, K. Olejník, P. Malý, R. P. Campion, B. L. Gallagher, J. Sinova, and T. Jungwirth, *Nature* 4 (2013) 1422.
- [2] T. Dietl, and H. Ohno, *Review of Modern Physics* 86 (2014) 187.
- [3] A. W. Rushforth, E. De Ranieri, J. Zemen, J. Wunderlich, K. W. Edmonds, C. S. King, E. Ahmad, R. P. Campion, C. T. Foxon, B. L. Gallagher, K. Výborný, J. Kučera, and T. Jungwirth, *Physical Review B* 78 (2008) 085314.
- [4] A. Lemaître, A. Miard, L. Travers, O. Mauguin, L. Largeau, C. Gourdon, V. Jeudy, M. Tran, and J.-M. George. *Applied Physics Letters* 93 (2008) 021123.
- [5] K. Olejník, M. H. S. Owen, V. Novák, J. Mašek, A. C. Irvine, J. Wunderlich, and T. Jungwirth, *Physical Review B* 78 (2008) 054403.
- [6] A. V. Kimel, G. V. Astakhov, G. M. Schott, A. Kirilyuk, D. R. Yakovlev, G. Karczewski, W. Ossau, G. Schmidt, L. W. Molenkamp, and T. Rasing, *Physical Review Letters* 92 (2004) 237203.
- [7] G. V. Astakhov, A. V. Kimel, G. M. Schott, A. A. Tsvetkov, A. Kirilyuk, D. R. Yakovlev, G. Karczewski, W. Ossau, G. Schmidt, L. W. Molenkamp, and Th. Rasing, *Applied Physical Letters* 86 (2005) 152506.
- [8] Y. Hashimoto and H. Munekata, *Applied Physical Letters* 93 (2008) 202506.
- [9] P. Němec, E. Rozkotová, N. Tesařová, F. Trojánek, E. De Ranieri, K. Olejník, J. Zemen, V. Novák, M. Cukr, P. Malý, and T. Jungwirth, *Nature Physics* 8 (2012) 411- 415.
- [10] M. Bombeck, A. S. Salasyuk, B. A. Glavin, A. V. Scherbakov, C. Brüggemann, D. R. Yakovlev, V. F. Sapega, X. Liu, J. K. Furdyna, A. V. Akimov, and M. Bayer, *Physical Review B* 85 (2012) 195324.
- [11] L. Thevenard, E. Peronne, C. Gourdon, C. Testelin, M. Cubukcu, E. Charron, S. Vincent, A. Lemaître, and B. Perrin, *Physical Review B* 82 (2010) 104422.
- [12] L. Thevenard, J.-Y. Duquesne, E. Peronne, H. J. von Bardeleben, H. Jaffres, S. Ruttala, J.-M. George, A. Lemaître, and C. Gourdon, *Physical Review B* 87 (2013) 144402.
- [13] L. Thevenard, C. Gourdon, J. Y. Prieur, H. J. von Bardeleben, S. Vincent, L. Becerra, L. Largeau, and J.-Y. Duquesne, *Physical Review B* 90 (2014) 094401.
- [14] J. Zemen, J. Kucera, K. Olejník, and T. Jungwirth, *Physical Review B* 80 (2009) 155203.
- [15] M. Glunk, J. Daeubler, L. Dreher, S. Schwaiger, W. Schoch, R. Sauer, W. Limmer, A. Brandlmaier, S. T. B. Goennenwein, C. Bihler and M. S. Brandt, *Physical Review B* 79 (2009) 195206.
- [16] W. Li, P. Dhagat, and A. Jander, *IEEE Trans. Magn* 48 (2012) 4100.
- [17] W. Li, B. Buford, A. Jander, and P. Dhagat, *Journal of Applied Physics* 115 (2014) 17E307.
- [18] S. Davis, J. A. Borchers, B. B. Maranville, and S. Adenwalla, *Journal of Applied Physics* 117 (2015) 063904.
- [19] A. Hubert and R. Schäfer, *Magnetic domains*, Springer, Berlin (2009).
- [20] A. K. Zvezdin and V. A. Kotov, *Modern magneto-optics and magneto-optical materials*, *Studies in Condensed Matter Physics*, Taylor & Francis Group (New York), 1997.
- [21] C. Sun, J. Kono, Y. -H. Cho, A. K. Wojcik, A. Belyanin, and H. Munekata, *Physical Review B* 83 (2011) 125206.
- [22] A. Dourlat, V. Jeudy, C. Testelin, F. Bernardot, K. Khazen, C. Gourdon, L. Thevenard, L. Largeau, O. Mauguin, and A. Lemaître, *Journal of Applied Physics* 102 (2007) 023913.
- [23] K. Nakamura, T. Asaka, S. Asari, Y. Ota, and A. Itoh, *IEEE Transactions on Magnetism* MAG-21 (1985) 1654.

- [24] P. H. Lissberger, *Journal of the Optical Society of America* 51 (1961) 948, and references therein.
- [25] K-M. Wu, J-F. Wang, K-C. Chen, J-C. Wu, and L. Horng. *Journal of Magnetism and Magnetic Materials* 310 (2007) e944–e946.
- [26] L. Thevenard, L. Largeau, O. Mauguin, G. Patriarche, and A. Lemaître, *Physical Review B* 73 (2006) 195331.
- [27] K. Sato, *Japanese Journal of Applied Physics* 20,(1981) 2403-2409.
- [28] I. H. Malitson, *Journal of the Optical Society of America* 55, (1965) 1205.

## Figure captions

Fig.2. Kerr rotation spectra at different temperatures for GaMnAs (a) and GaMnAs/SiO<sub>2</sub> (b) layers.

Fig.2. Ellipticity as a function of wavelength at  $T=10$  K for GaMnAs (black empty circles) and GaMnAs/SiO<sub>2</sub> (red squares).

Fig.3. Snapshots of the magnetic domain structure observed by KM in a temperature range 30 K - 90 K, on the GaMnAs layer with and without SiO<sub>2</sub> capping layer (right and left side of the dashed line, respectively). The sample edge is shown by a full line. Here, the magnetic contrast has been digitally enhanced with respect to the original images for the sake of clarity.

Fig.4. Dependence of the Kerr rotation peak amplitude (open circles) and the magnetic contrast of Kerr images (solid squares) on the temperature for GaMnAs (a) and GaMnAs/SiO<sub>2</sub> (b) layers.

Fig.5. Schematic illustration of a model based on optical interferences in (Ga,Mn)As/SiO<sub>2</sub> structure. For the sake of clarity, the experimentally near-normal incidence light beam is shown here with a large incidence angle.

Fig. 6. Reflectance as a function of SiO<sub>2</sub> thickness at the peak of Kerr rotation ( $\lambda=704$  nm), for normal incidence (full line) and 20° incidence (dashed line). The dotted vertical line shows the value of the SiO<sub>2</sub> thickness equal to a quarter wavelength in the SiO<sub>2</sub> layer  $e=\lambda/(4n_1)$ . The inset shows the SiO<sub>2</sub> thickness for minimum reflectance as a function of the wavelength (Eq. 2).

Fig. 7. Kerr rotation angle (solid line) and ellipticity (dashed-dotted line) at 704 nm (peak of the Kerr rotation) and  $T=10$ K as a function of the SiO<sub>2</sub> thickness from Eq. 3. The arrows show the change of Kerr rotation and ellipticity from no SiO<sub>2</sub> layer to a 80 nm SiO<sub>2</sub> layer.